Meat and Muscle Biology™


# Daily Quantification of Myoglobin Forms on Beef *Longissimus Lumborum* Steaks Over 7 Days of Display by Near-infrared Diffuse Reflectance Spectroscopy[a]

Daqing Piao[1]*, Morgan L. Denzer[2], Gretchen Mafi[2], and Ranjith Ramanathan[2]

[1]School of Electrical and Computer Engineering, Oklahoma State University, Stillwater, OK 74078, USA
[2]Department of Animal Sciences, Oklahoma State University, Stillwater, OK 74078, USA
[a]This research was supported, in part, by the Leo & Kathy Noltensmeyer Endowed Research Professorship to Ranjith Ramanathan and the Division of Agricultural Sciences and Natural Resources at Oklahoma State University.
Declarations of interest: none.
*Corresponding author. Email: daqing.piao@okstate.edu (Daqing Piao)

**Abstract:** Near-infrared diffuse reflectance spectroscopy (NIR-DRS) was utilized to develop an algorithm using approximately 18 wavelengths spanning 480 to 650 nm to determine oxymyoglobin (OxyMb), deoxymyoglobin (DeoxyMb), and metmyoglobin (MetMb) contents on beef *longissimus lumborum* muscles. Daily changes in subsurface myoglobin redox forms were evaluated for 7 d using NIR-DRS and compared with the surface color as assessed by a HunterLab MiniScan spectrophotometer as a reference modality. Both measurements revealed that MetMb increased steadily over the duration of display, showing high correlation ($R^2 = 0.91$) between the 2 methods. Comparatively, whereas NIR-DRS revealed OxyMb to have decreased steadily over the period of display, the HunterLab MiniScan spectrophotometer indicated a much later onset of the apparent decrease of OxyMb, resulting in a moderate correlation ($R^2 = 0.64$) between the 2 methods. No correlation was found between the 2 methods regarding the changes of DeoxyMb over the duration of display. The newly developed NIR-DRS algorithm has potential as an alternative method of color assessment in postrigor skeletal muscle.

**Key words:** meat color, diffuse reflectance spectroscopy, reflecto-spectrophotometry, myoglobin
*Meat and Muscle Biology* 5(1): 42, 1–14 (2021) **doi:10.22175/mmb.12562**
Submitted 6 May 2021 Accepted 6 September 2021

## Introduction

Meat color is an important sensory attribute that influences purchasing decisions. Meat color depends on the concentration and oxidation status of myoglobin (Mancini and Hunt, 2005). Myoglobin is the primary sarcoplasmic protein responsible for meat color. In fresh meat, myoglobin can exist in any of the 3 redox states: oxymyoglobin (OxyMb), deoxymyoglobin (DeoxyMb), and metmyoglobin (MetMb). Predominant OxyMb form on the meat surface, giving a consumer-preferred bright cherry-red color, whereas the color of DeoxyMb is purplish-red, commonly seen in the interior of a freshly cut steak or vacuum-packaged meat. The formation of brown-colored MetMb on the surface of beef products results from the oxidation of ferrous OxyMb and/or DeoxyMb (Ramanathan et al., 2019). Therefore, quantification of myoglobin redox forms on the surface of meat is of utmost importance for researchers and industry.

The 3 redox forms of myoglobin strongly but unequally absorb light in the visible spectrum when compared with other light-absorbing molecules in meat, such as water or fat (Bowen, 1949). Hence, spectrally distinct absorption features of myoglobin redox states establish the basis for reflectance and absorbance-based quantification of myoglobin concentration in muscle (Wilson et al., 1989). Because of the similarity of the heme-moiety, both hemoglobin and myoglobin have similar spectral characteristics

(Davis and Barstow, 2013). However, hemoglobin proportion in muscle is usually quite small (de Groot et al., 1999); hence, the effect of hemoglobin on myoglobin quantification is often neglected.

Muscle has a unique matrix that allows light to be absorbed, reflected, scattered, and transmitted (Hughes et al., 2019). Whichever approach is used to probe the myoglobin-dominating spectral absorption of light by muscle to quantify myoglobin redox states via surface assessment, the operation has generally involved the following sequences (Swatland, 2008; Hughes et al., 2017; Purslow et al., 2020):

1. Light of spectral components—either broad-band or at discrete wavelengths that span the isobestic interests—are delivered to the muscle via free-space optics or alternatively fiberoptical means for contact applications that could, in principle, also be delivered by noncontact means between the applicator and the muscle.
2. A small portion (~4%) of incident light is reflected by the muscle surface (specular reflection), owing to the refractive index mismatch between the light-delivery conduit (air when delivered in free-space or optical fiber when delivered for muscle contact) and the bulk of muscle.
3. A greater portion of the incident light than that of specular reflection penetrates into the muscle and interacts with scatterers such as muscle fiber and absorbers, including myoglobin of various redox forms, causing the light to diffuse in the muscle to make the intensity to reduce rapidly (at a rate faster than exponential decay) as the line-of-sight propagation distance increases.
4. Some of the light diffusely propagated in muscle reaches the surface and escapes to become diffuse reflectance (remission of light at microscopic positions overlapping with or offset from the site of illumination) that is inseparable from the surface specular reflection based on the intensity patterns alone.
5. The spectral profile of the diffuse reflectance is implemented in a mathematical model to recover the lumped absorption spectral profile corresponding to the total amount of absorption by all absorbers in muscle, the accuracy of which is also dependent upon the spectral variation of muscle scattering.
6. The lumped absorption profile is implemented in a second mathematical model to deduce the percentages of the individual myoglobin forms or to first reconstruct the molar concentration of the individual myoglobin forms and then to calculate the percentages of the individual myoglobin forms.

The American Meat Science Association (AMSA) recommends 2 methods or algorithms for deducing the myoglobin forms (Hernandez et al., 2015) using surface diffuse reflectance measurements. One of the 2 algorithms is based on the popular Kubelka-Munk (KM) theory of reflectance under diffuse illumination (Kubelka, 1948; Molenaar et al., 1999; Mourant et al., 2014; Sandoval and Kim, 2014). Among the various approaches of quantifying absorption properties based on the KM theory, a simplest method is to relate the wavelength-dependent light reflectance $R(\lambda)$ to a single wavelength-dependent KM function, denoted as $\frac{K}{S}(\lambda)$, by a concise model: $\frac{K}{S}(\lambda) = [1 - R(\lambda)]^2/[2R(\lambda)]$. The $\frac{K}{S}(\lambda)$ values at 4 isobestic wavelengths of $\lambda = 474$, 525, 572, and 610 nm are then combined to calculate the percentage of OxyMb, DeoxyMb, and MetMb with the values of the 3 summing up to 100%. The other of the 2 algorithms converts the wavelength-dependent light reflectance $R(\lambda)$ to wavelength-dependent absorbance, denoted as A $(\lambda)$, by a reflex attenuance model of A $(\lambda) = log[R(\lambda)]^{-1}$. The absorbances at 4 wavelengths (3 isobestic and 1 reference) of $\lambda = 474$, 525, 572, and 730 nm are then used to calculate the concentration of the 3 myoglobin types based on their known molar absorbance, from which the percentage of OxyMb, DeoxyMb, and MetMb are calculated with the values of the 3 summing up to 100%.

We note that, either of these 2 algorithms is implemented at the last 2 steps of the sequences summarized heretofore upon the acquisition of diffuse reflectance from the muscle. Regarding the first algorithm, how accurate the myoglobin form estimation can become is bounded by the robustness of the model of single-parameter KM theory to relate the single wavelength-dependent KM function $\frac{K}{S}(\lambda)$ to the measured diffuse reflectance $R(\lambda)$. A recent report (Piao and Sun, 2021) has challenged the robustness of the KM function $\frac{K}{S}(\lambda)$ in modeling the diffuse reflectance from a medium of the absorption significantly greater than the scattering, a tissue condition that is relevant to myoglobin form identification in muscle owing to the inherent need to sense at wavelengths strongly absorbed by myoglobin. Regarding the second algorithm, the main hypothesis (Hernandez et al., 2015) has been that myoglobin forms do not contribute to the reflectance, and thus to the reflex attenuance, at

730 nm. This hypothesis leads to the use of the reflex attenuance at 730 nm as a reference to the reflex attenuance assessed at 3 other wavelengths. Although appearing to be highly correlated, noticeable mismatch between the 2 algorithms applied to the same set of reflectance measurement was observed when estimating the absolute values of myoglobin form proportions. Arguably, these model limitations indicate that myoglobin form estimation by the existing popular algorithms is certainly convenient but might not be conclusive. This entails exploration of new algorithmic approaches to optimizing information extraction from existing measurements of muscle reflectance or further development of novel instrument methods to assess the myoglobin form of muscle.

In the present research, we developed an in-house near-infrared diffuse reflectance spectroscopy (NIR-DRS) with the method of probing the muscle differently than the popular methods that have been accommodated with the AMSA recommended algorithms. This NIR-DRS was configured using an applicator probe allowing a sampling depth of approximately 1.5 mm, deeper than that rendered by the current spectrophotometer approaches. The diffuse reflectance acquired by this deeper-probing probe from the muscle containing the myoglobin absorption information is then processed at approximately 18 wavelengths to quantify the myoglobin redox states. It is worth noting that, the current research utilized 18 wavelengths spanning the absorption maxima of the 3 redox forms of myoglobin, which would make the quantification potentially more accurate than the currently implemented ones involving no more than 4 wavelengths.

# Materials and Methods

Muscles samples were obtained from a USDA inspected beef processing facility. Hence, this research did not require that the Animal Care and Use Protocol be approved by the Institutional Animal Care and Use Committee of Oklahoma State University.

## *Raw materials, processing, and retail display*

Eight USDA Choice strip loins (*longissimus lumborum*; Institutional Meat Purchase Specifications #180) were purchased from a major packing facility 3 d postmortem (grain-fed, market-age cattle). Vacuum-packaged loins were transported on ice to the Robert M. Kerr Food and Agricultural Products Center at Oklahoma State University. On day 5 postmortem, six 2.5-cm-thick steaks were cut perpendicular to muscle fiber orientation using a meat slicer (Bizerba USA Inc., Piscataway, NJ). The overall goal was to compare color measurements between 2 instrument methods. The loins were vacuum packaged. Freshly cut surface was utilized for the study without any discoloration. The first steak was used to measure surface color using NIR-DRS and a HunterLab MiniScan spectrophotometer, the second through fourth steaks were used to prepare each myoglobin form according to the AMSA color guide to be used as the myoglobin form standards, the fifth steak was used to measure pH, and the sixth steak was used to determine proximate composition. The steaks assigned for surface color measurements were placed onto foam trays with absorbent pads, overwrapped with oxygen-permeable polyvinyl chloride (PVC) fresh meat films (15,500 to 16,275 $cm^3$ $O^2/m^2$ per 24 h at 23°C; E-Z Wrap Crystal Clear Polyvinyl Chloride Wrapping Film, Koch Supplies, Kansas City, MO). After packaging, steaks were placed in a coffin-style open display case maintained at 2°C ± 1°C under continuous lighting (1,612 to 2,152 lux; Philips Deluxe Warm White Fluorescent lamps; Andover, MA; color rendering index = 86; color temperature = 3,000° K). All packages were rotated daily to minimize the effects of variation in light intensity or temperature due to location.

## *Proximate and pH determinations*

The pH of steaks was measured on day 5 postmortem. Ten grams of the steak samples were blended with 100 mL of deionized water at 25°C and then homogenized for 30 s in a Sorvall Omni tabletop mixer (Newton, CT). The pH of the muscle homogenates was measured using an Accumet combination glass electrode connected to an Accumet 50 pH meter (Fisher Scientific, Fairlawn, NJ). Proximate compositions were determined by an AOAC-approved FOSS FoodScan™ 78800 near-infrared spectrophotometer (Dedicated Analytical Solutions, Hillerod, Denmark). Moisture, protein, and fat composition were recorded on a percentage basis.

## *Color measurement by using HunterLab MiniScan spectrophotometer*

The steaks assigned to surface color were utilized for both the HunterLab MiniScan spectrophotometer and NIR-DRS. The surface color was measured on the steaks at 3 random locations using a HunterLab MiniScan XE Plus spectrophotometer (HunterLab Associates, Reston, VA) with a 2.5-cm-diameter

aperture, illuminant A, and 10° standard observer, shortly prior to the measurement using the NIR-DRS system. Values for CIE $L^*$, $a^*$, and $b^*$ (Illuminant A) were collected, and hue angle (tan_1 $b^*/a^*$) and chroma $(a^{*2} + b^{*2})^{1/2}$ were calculated (Hunt, 1991) from instrumental measures. We note that the raw spectral profile acquired by HunterLab on the surface of steaks was the wavelength-dependent reflectance (R) at wavelengths from 400 to 700 nm at a 10 nm spectral interval. This reflectance $R(\lambda)$ from 400 to 700 nm at 10 nm spectral spacing was output to a computer program to obtain $R(\lambda)$ at 4 isobestic wavelengths of $\lambda = 474$, 525, 572, and 610 nm by interpolation when needed. The $R(\lambda)$ at the 4 isobestic wavelengths were then converted to $\frac{K}{S}(\lambda)$ at the corresponding wavelengths, for substituting into the appropriate equations (AMSA, 2012) to calculate the percentage of OxyMb, DeoxyMb, and MetMb with the values of the 3 summing up to 100%.

### *Near-infrared diffuse reflectance spectroscopy*

NIR-DRS of the steaks was acquired using a device shown schematically and photographed in Figure 1. The NIR-DRS device was custom developed in the laboratory (Piao et al., 2018). Specifically, the output of a Halogen light source (Cuda I-150; Jacksonville, FL) through a fiberoptical light conduit of 6 mm in core diameter was coupled by a 40 × achromatic objective lens (Olympus RMS40X; Thorlabs Inc., Newton, NJ) onto a 400-µm fiber near the center of an in-house

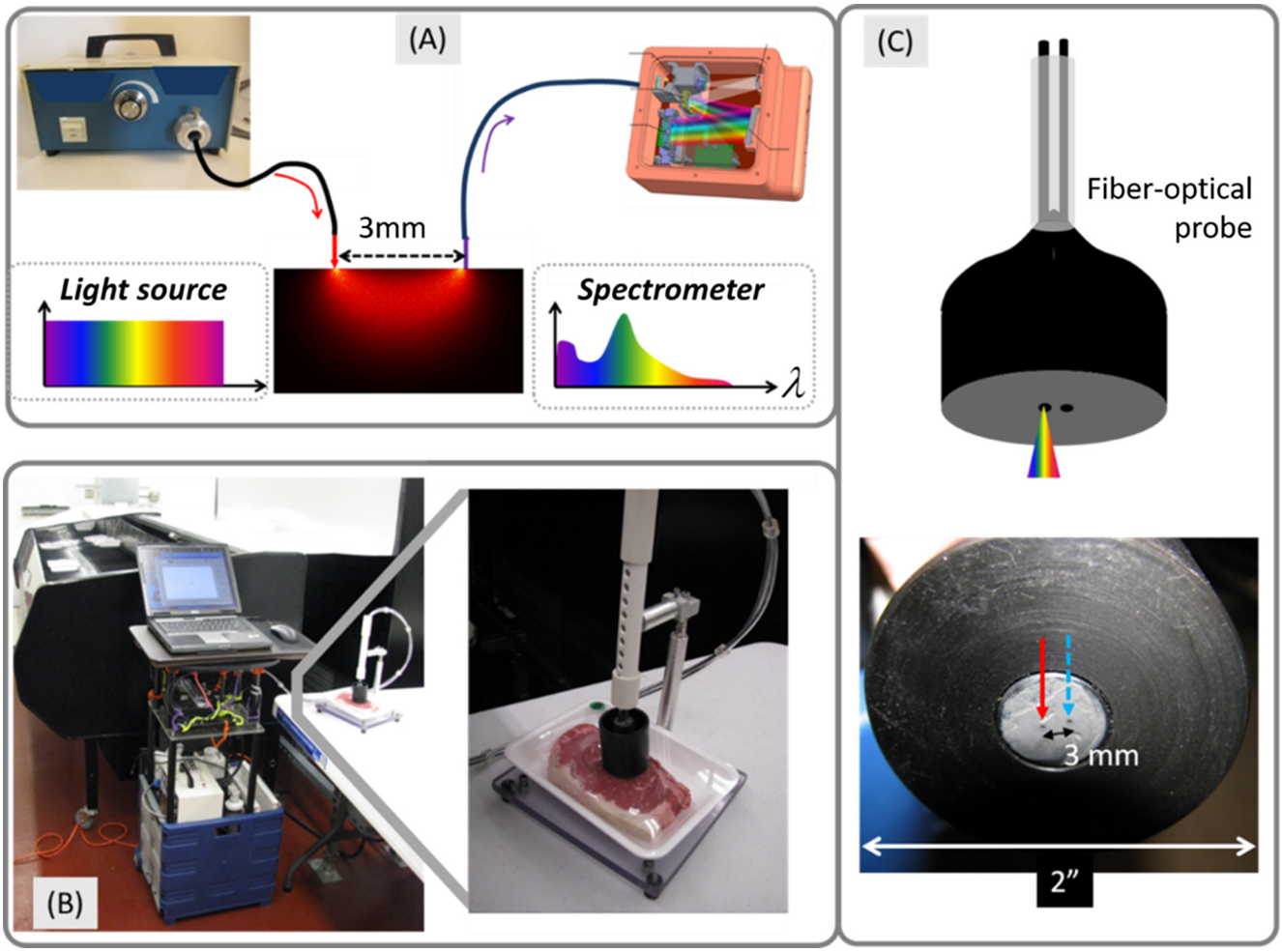


**Figure 1.** A lab-on-a-crate NIR diffuse-reflectance spectroscopy system used for assessing the changes of myoglobin form over the days of display. (A) Schematic of the near-infrared spectroscopy where a broad-band light source is incident via a fiber to sample, and the light diffusely propagated in the sample is collected by another fiber placed 3 mm in distance from the illuminating fiber. (B) The lab-on-a-crate near-infrared spectroscopy system placed by the open display case. The inset shows the applicator probe placed on the sample surface. (C) Schematic of the applicator probe. Two 400-µm fiber were fabricated at 3 mm separation into a two-part holder that combined to make a probe of 2” in diameter. One fiber illuminates, i.e., illuminates light, and the other one collects light diffusely propagated in the sample when the probe is pressed on the sample surface so no surface reflection is acquired.

developed applicator probe of 2" in diameter as the source fiber for illuminating muscle. A second 400-μm fiber on the same applicator probe and at a 3-mm separation from the illumination fiber collected light diffusely propagated through the muscle when the applicator probe was brought in contact with PVC-wrapped muscle and stabilized by the weight of the probe itself. The 3-mm source-detector separation of the applicator probe corresponded to an approximate sampling depth of 1.5 mm. The detector fiber was coupled to a compact visible/near-infrared spectrometer (NT58-303; Edmund Optics Inc., Barrington, NJ) having a 16-bit data resolution (0-65535) that was controlled by a laptop computer via a vendor-provided user interface. The acquired raw spectral profile was saved to a text format compatible with Microsoft Excel (Redmond, WA) for off-line processing in MATLAB environment. The effective spectral response of the system was approximately 400 to 900 nm; however, only the spectra over 480 to 650 nm were processed as they were limited by the availability of the spectral absorbance of OxyMb, DeoxyMb, or MetMb to be used with the algorithm.

The daily measurement of the muscle by using DRS was performed at near 24-h intervals from day 0 to day 7 of the display. At each time of the day for daily measurement, the DRS system was turned on to warm up for approximately 20 min. Reference DRS spectra for quality check were then acquired from a set of 3 solid phantoms having nearly identical scattering properties and absorption properties that scaled at approximately 1:2:4 (Piao, 2019). Each steak was then brought to be placed in hands-free contact with the applicator probe. DRS spectra were obtained at 3 random sites (2 near the opposite ends of the length and 1 at the middle section) of the steak at positions roughly consistent with those assessed immediately previously with the HunterLab MiniScan spectrophotometer. All DRS raw spectra were acquired at an acquisition time of 100 ms and averaged over 5 acquisitions at each position.

The raw DRS spectra profile was post-processed to remove the effect of source-spectral variation as well as baseline noise which was acquired by placing the 2" handheld probe on a thick dark cloth under normal ambient lighting. The noise-deducted spectral reflectance was then normalized with respect to the noise-deducted spectral reflectance of a reflective standard of 10% surface reflectivity (LabSphere) placed at a distance of approximately 2 mm to collect the native spectrum of the light source. The normalized spectral reflectivity of muscle was modeled by a formula accounting for the attenuation by the muscle due to absorption and scattering properties over the 3 mm source-detector separation (Sun and Piao, 2019). The muscle scattering was assumed to be wavelength invariant over the spectrum of interest (480 to 650 nm) (Schmitt and Kumar, 1998), which allowed us to calculate the total spectral absorption of muscle from the normalized spectral reflectance. The muscle's spectral absorption was assumed to be dominated by the 3 redox forms of myoglobin, OxyMb, DeoxyMb, and MetMb (de Groot et al., 1999; Mohan et al., 2010a). The absorption of each myoglobin form was the product of the molar extinction coefficient and the molar concentration. When the number of wavelengths at which the absorption measurement was available was not less than the number of unknowns, i.e., 3 here for the concentrations of the 3 forms of myoglobin, linear inversion of spectral absorption for spectral decomposition was rendered by way of matrix manipulation. The spectral decomposition then gave the volume proportion (percentage) of the 3 redox forms. In this work, we utilized the DRS measured at 18 wavelengths, from 480 to 650 nm at a wavelength interval of 10 nm, to resolve the 3 redox forms of myoglobin.

### *Estimation of the absorbance of myoglobin redox states at a 10 nm spectral interval over 480 to 650 nm from literature data*

We note that the raw spectral measurement taken by the HunterLab MiniScan spectrophotometer from the muscle had a spectral coverage of 400 to 700 nm and a wavelength spacing of 10 nm, i.e., at wavelengths of 410 to 700 nm, whereas the raw spectral measurement taken by NIR-DRS had a spectral coverage wider than 400 to 700 nm and a sub-nanometer spectral resolution. To assess how well NIR-DRS may resolve myoglobin redox states providing the same level of raw instrument information accessible from the muscle, it became imperative to assume that NIR-DRS acquisition of the reflectance from the muscle was over the same spectral range and at the same wavelength spacing as rendered by the HunterLab MiniScan spectrophotometer. This would imply the need to implement spectral decomposition at a spectral spacing of 10 nm. To do this, however, would require knowing the extinction coefficient of the myoglobin redox forms over 400 to 700 nm with the spectral resolution specified at 10 nm. To our knowledge, there was no known database of such. We thus developed an alternative approach to estimate the extinction coefficients—or, equivalently, the absorbances of OxyMb, DeoxyMb, and MetMb—by using a set of data

published by Tang et al. (2004) containing the absorbance of OxyMb, DeoxyMb, and MetMb measured over a 1-cm pathlength over a spectral range of approximately 475 nm to 650 nm.

The following procedures were implemented to estimate the absorbance of OxyMb, DeoxyMb, and MetMb from 480 nm to 650 nm at a wavelength spacing of 10 nm. (1) Figure 1 of Tang et al., 2004 was magnified and overlapped with a grid having a wavelength spacing of 10 nm covering 480 to 650 nm and an absorbance spacing of 2.5. The overlapped grid allowed for estimating the absorbance of OxyMb, DeoxyMb, MetMb at the wavelength starting at 480 nm with a spacing of 10 nm. The absorbances of OxyMb, DeoxyMb, and MetMb estimated as such were replotted over the same scales as in the work by Tang et al. (2004)—as shown in Figure 2A—and fine-tuned, until the curves by estimation were visually consistent with those of the original Figure 1 of Tang et al. (2004). (2) The utility of the reproduced absorbance of the 3 myoglobin forms shown in (A) can be appreciated by noticing the evaluation of the spectral profiles measured from one muscle sample (#3) over the duration of display, as shown in Figure 2B. The 2 valleys centered around 540 nm and 580 nm clearly were the spectral markers of OxyMb, which became less pronounced as the display progressed that indicated the reduction of OxyMb over the duration of display. Comparatively, the spectral intensity around 635 nm reduced steadily, which would correspond to increased absorption due to the increase of MetMb formation over the duration of display. The absorbance at the specific wavelengths spaced at 10 nm, denoted as $A(\lambda)$, could then be converted to absorption coefficient in ($cm^{-1}$) by $\mu_a(\lambda) = 2.303\ A(\lambda)$, from which the molar extinction coefficient can be calculated according to the molar weight of myoglobin. Given the same molar weight of the 3 redox forms of myoglobin, the ratio of their extinction coefficients will be represented by the ratio of the absorption coefficients or absorbances. Therefore, the spectral absorption converted from the DRS measured spectral reflectance was used in the final quantification of the myoglobin redox forms.

## Statistical analysis

The experimental design was a randomized complete block. Loin from each animal served as a block, i.e., each

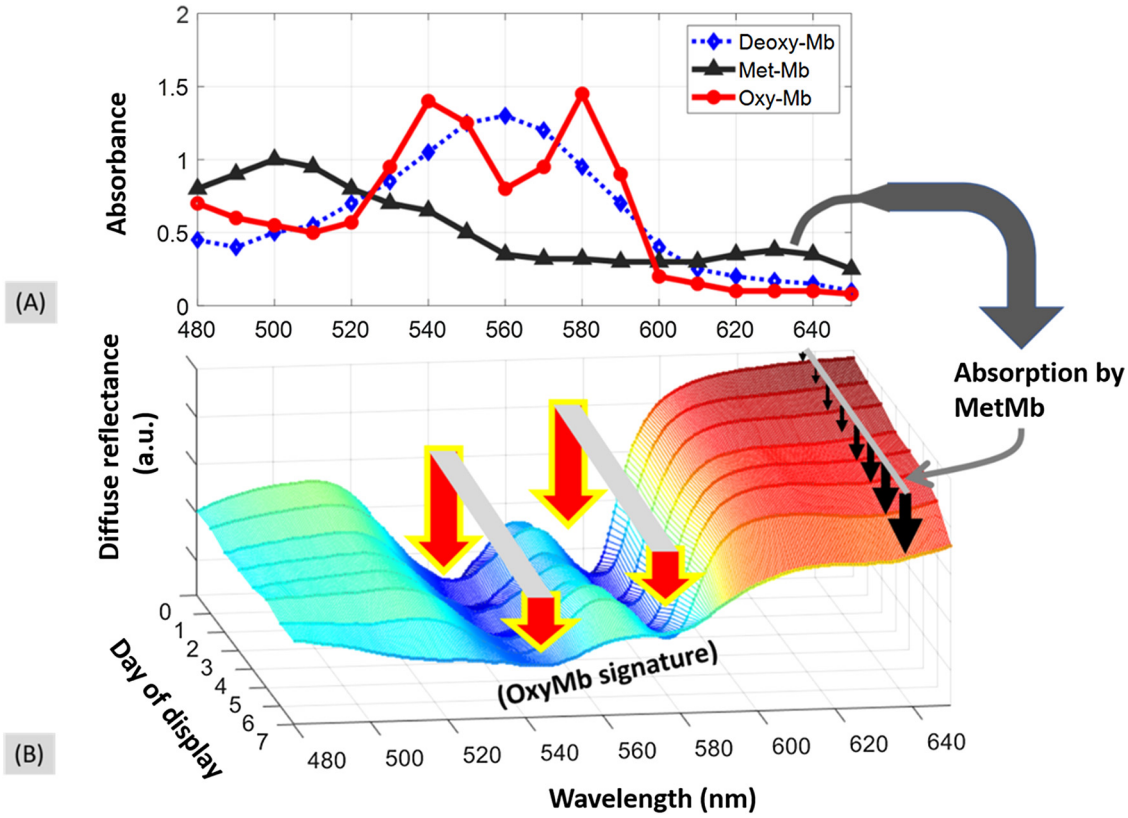


**Figure 2.** (A) Absorbance of OxyMb, DeoxyMb, and MetMb at a 10-nm spectral resolution starting from 480 nm to 650 nm, as estimated by using the 480 to 650 nm spectral range figure 1 of Tang et al. (2004). (B) Sample traces of normalized diffuse reflectance acquired from the same muscle over the d 0 to d 7 and over 480 to 650 nm show the changes caused by the expected reduction of OxyMb as marked by the red framed arrows and increase of MetMb as marked by the dark simple arrows.

loin was used as a random term. Display time was the main treatment effect. Data were analyzed separately for each variable (OxyMb, DeoxyMb, and MetMb). Multiple NIR-DRS scans on each steak (3 per steak) were averaged for statistical analysis. To assess the strength of relationships between HunterLab MiniScan spectrophotometric and NIR-DRS measurements, simple correlation coefficients between the results of the 2 methods were computed using commands available in MATLAB.

# Results and Discussion

## *pH and proximate composition*

The pH and proximate compositions are included in Table 1. All loins were from the normal-pH range.

**Table 1.** The mean and standard error (SE) for pH, fat, protein, and moisture of loins used in the study

| Trait | Mean ± SE |
|---|---|
| pH | 5.51 ± 0.01 ($n$ = 24) |
| Fat (%) | 9.58 ± 0.69 ($n$ = 16) |
| Protein (%) | 22.18 ± 0.18 ($n$ = 16) |
| Moisture (%) | 67.46 ± 0.59 ($n$ = 16) |

The parentheses after each SE indicates the sample size.

## *Daily intermuscle variation of OxyMb, DeoxyMb, and MetMb forms as measured by DRS versus HunterLab MiniScan spectrophotometer*

The day-to-day changes of the myoglobin redox forms of all 8 muscles over the duration of display are collectively presented as two-dimensional maps in Figure 3. The upper panel, consisting of subplots (A), (B), and (C), was the result estimated by DRS. The lower panel, consisting of subplots (D), (E), and (F), was the result of assessment by HunterLab MiniScan spectrophotometer, which lacked the data on day 4 because of technical issues. On each sub-figure, the column corresponds to the day of measurement spanning from day 0 to day 7, and the row corresponds to the number of the sample among the 8 muscles. The two-dimensional image helps assess intermuscle variation of OxyMb measured by DRS in (A) and by HunterLab in (D), similarly for DeoxyMb in (B) and (E) and for MetMb in (C) and (F), on each day of the duration of display. The OxyMb, DeoxyMb, and MetMb are all displayed at the same color scale from 0% to 100%. A deep blue indicated a low level approaching 0%, whereas a bright red indicated a high level toward 100%.

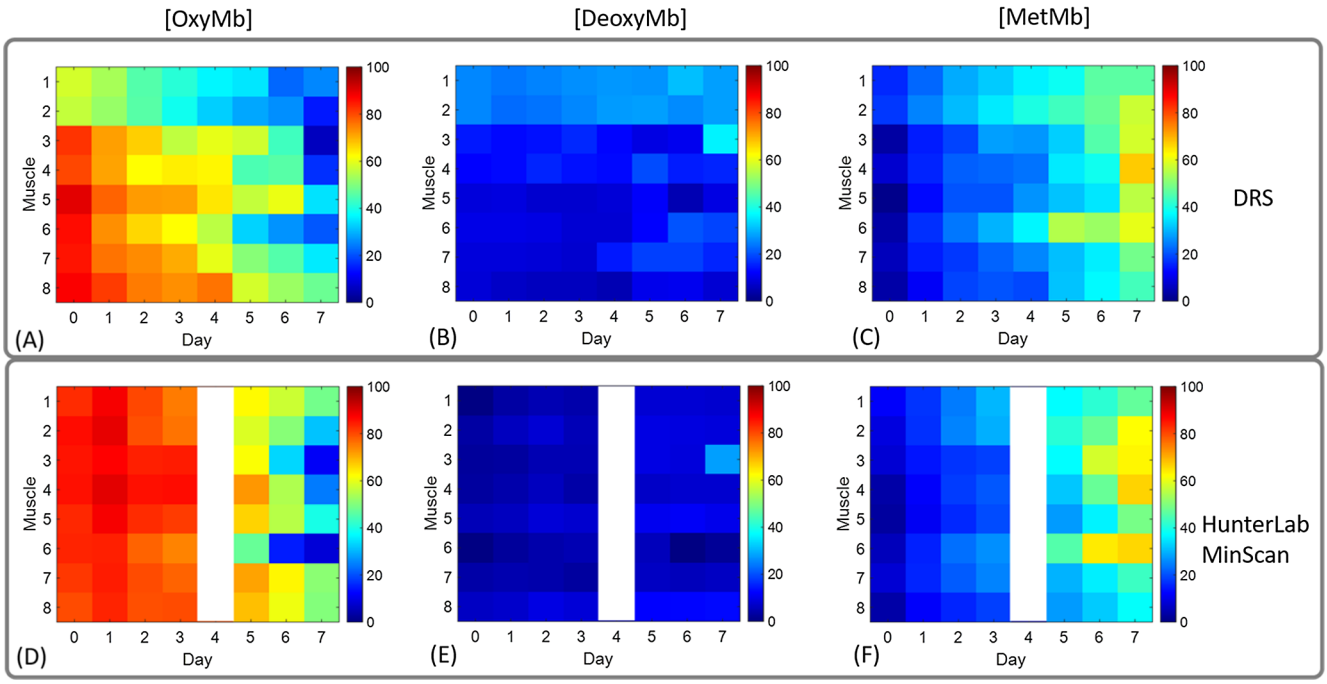


**Figure 3.** Intersample variations of OxyMb, DeoxyMb, and MetMb of the 8 muscles over the duration of display. The upper panel consisting of subplots (A), (B), and (C) was the result of DRS. The lower panel consisting of subplots (D), (E), and (F) was the result of HunterLab. On each sub-figure, the column corresponds to the day of measurement that spans from day 0 to day 7, and the row corresponds to the sample number out of 8 muscles. OxyMb estimation is depicted in (A) and (D), DeoxyMb estimation is depicted in (B) and (E), and MetMb estimation is depicted in (C) and (F). All traits, including OxyMb, DeoxyMb, and MetMb, are displayed at the same color scale corresponding to 0%–100%. Blue indicates lower percentage, whereas red indicates higher percentage.

The ranges of OxyMb of the 8 muscles are tabulated in Table 2A, with the upper-half panel corresponding to those assessed by NIR-DRS and the lower-half panel corresponding to those assessed by HunterLab MiniScan spectrophotometer. The ranges of DeoxyMb of the 8 muscles are tabulated in Table 2B, where the upper-half panel corresponds to those assessed by NIR-DRS and the lower-half panel corresponds to those assessed by HunterLab MiniScan spectrophotometer. The ranges of MetMb of the 8 muscles are tabulated in Table 2C, with the upper-half panel represents those assessed by NIR-DRS and the lower-half panel represents those assessed by HunterLab MiniScan spectrophotometer.

From these two-dimensional mappings, the following trends may be appreciated regarding the muscle color change over the duration of display from day 0 to day 7 when excluding day 4:

1. OxyMb and DeoxyMb as estimated by DRS showed greater intersample variations when compared with those estimated by HunterLab MiniScan spectrophotometer. The OxyMb and DeoxyMb of samples 1 and 2 were perceivably lower than those of the remaining 6 samples over the most part of day 0 to day 7, when estimated by DRS.
2. OxyMb levels decreased gradually over the days when estimated by DRS as well as by HunterLab MiniScan spectrophotometer. However, the onset of the decrease seemed to have occurred later when estimated by HunterLab MiniScan spectrophotometer than when estimated by DRS.
3. MetMb levels increased gradually over the days when estimated by both DRS and HunterLab MiniScan spectrophotometer.
4. The change of Deoxy levels over the duration of the display was much less remarkable than that of

**Table 2A.** Daily intermuscle variation of OxyMb measured by NIR-DRS (upper-half panel) and HunterLab MiniScan spectrophotometer (lower-half panel)

| | Day 0 | Day 1 | Day 2 | Day 3 | Day 4 | Day 5 | Day 6 | Day 7 |
|---|---|---|---|---|---|---|---|---|
| **Maximum** | 90.2% | 81.4% | 75.2% | 73.4% | 75.8% | 58.2% | 60.2% | 48.0% |
| **Minimum** | 56.6% | 52.0% | 45.5% | 38.9% | 32.6% | 28.6% | 22.6% | 6.0% |
| | **Day 0** | **Day 1** | **Day 2** | **Day 3** | **Day 4** | **Day 5** | **Day 6** | **Day 7** |
| **Maximum** | 86.0% | 90.0% | 85.7% | 86.2% | | 72.3% | 63.1% | 51.0% |
| **Minimum** | 79.7% | 83.6% | 77.4% | 74.4% | | 47.3% | 14.9% | 8.6% |

NIR-DRS = near-infrared diffuse reflectance spectroscopy; OxyMb = oxymyoglobin.

**Table 2B.** Daily intermuscle variation of DeoxyMb measured by NIR-DRS (upper-half panel) and HunterLab MiniScan spectrophotometer (lower half-panel)

| | Day 0 | Day 1 | Day 2 | Day 3 | Day 4 | Day 5 | Day 6 | Day 7 |
|---|---|---|---|---|---|---|---|---|
| **Maximum** | 25.7% | 24.0% | 25.3% | 26.3% | 27.4% | 57.7% | 31.2% | 36.1% |
| **Minimum** | 8.4% | 6.9% | 5.9% | 6.2% | 5.0% | 9.6% | 4.7% | 8.1% |
| | **Day 0** | **Day 1** | **Day 2** | **Day 3** | **Day 4** | **Day 5** | **Day 6** | **Day 7** |
| **Maximum** | 6.4% | 7.2% | 9.6% | 8.2% | | 12.4% | 12.8% | 27.9% |
| **Minimum** | -0.2% | 2.5% | 4.1% | 3.0% | | 5.7% | -0.5% | 2.2% |

DeoxyMb = deoxymyoglobin; NIR-DRS = near-infrared diffuse reflectance spectroscopy.

**Table 2C.** Daily intermuscle variation of MetMb measured by NIR-DRS (upper-half panel) and HunterLab MiniScan spectrophotometer (lower-half panel)

| | Day 0 | Day 1 | Day 2 | Day 3 | Day 4 | Day 5 | Day 6 | Day 7 |
|---|---|---|---|---|---|---|---|---|
| **Maximum** | 17.8% | 25.0% | 30.5% | 35.4% | 40.1% | 54.8% | 52.6% | 67.3% |
| **Minimum** | 1.1% | 11.7% | 17.9% | 20.4% | 19.3% | 30.9% | 35.1% | 44.0% |
| | Day 0 | Day 1 | Day 2 | Day 3 | Day 4 | Day 5 | Day 6 | Day 7 |
| **Maximum** | 11.8% | 17.5% | 25.4% | 30.2% | | 45.6% | 64.3% | 66.5% |
| **Minimum** | 2.9% | 11.0% | 15.7% | 18.5% | | 27.4% | 32.3% | 37.9% |

MetMb = metmyoglobin; NIR-DRS = near-infrared diffuse reflectance spectroscopy.

**Table 3A.** The mean and standard error (SE) for OxyMb, DeoxyMb, and MetMb of 8 beef muscles measured by DRS during 7-d display

| | Day 0 | Day 1 | Day 2 | Day 3 | Day 4 | Day 5 | Day 6 | Day 7 |
|---|---|---|---|---|---|---|---|---|
| **OxyMb (%)** | 78.4 ± 2.7 | 69.6 ± 2.1 | 63.5 ± 2.2 | 59.7 ± 2.6 | 56.0 ± 2.8 | 45.5 ± 2.3 | 40.5 ± 2.6 | 25.3 ± 2.6 |
| **DeoxyMb (%)** | 14.3 ± 1.4 | 13.5 ± 1.2 | 13.8 ± 1.4 | 13.9 ± 1.6 | 14.6 ± 1.6 | 17.1 ± 1.4 | 17.2 ± 1.7 | 20.1 ± 1.9 |
| **MetMb (%)** | 7.4 ± 1.2 | 16.9 ± 0.9 | 22.7 ± 0.9 | 26.3 ± 1.1 | 29.4 ± 1.4 | 37.4 ± 1.6 | 42.3 ± 1.2 | 54.7 ± 1.5 |

The SE for each day is assessed over a sample size of 24 (8 muscles × 3 positions).

DeoxyMb = deoxymyoglobin; DRS = diffuse reflectance spectroscopy; MetMB = metmyoglobin; OxyMB = oxymyoglobin.

**Table 3B.** The mean and standard error (SE) for OxyMb, DeoxyMb, and MetMb of 8 beef muscles measured by HunterLab MiniScan during 7-d display

| | Day 0 | Day 1 | Day 2 | Day 3 | Day 4 | Day 5 | Day 6 | Day 7 |
|---|---|---|---|---|---|---|---|---|
| **OxyMb (%)** | 83.5 ± 0.4 | 87.0 ± 0.5 | 81.1 ± 0.6 | 79.4 ± 0.8 | -* | 63.7 ± 1.6 | 48.7 ± 3.1 | 33.1 ± 3.3 |
| **DeoxyMb (%)** | 3.0 ± 0.4 | 4.5 ± 0.3 | 6.2 ± 0.4 | 5.2 ± 0.3 | - | 8.7 ± 0.4 | 7.9 ± 0.8 | 10.5 ± 1.5 |
| **MetMb (%)** | 6.6 ± 2.9 | 14.4 ± 0.5 | 20.3 ± 0.7 | 23.6 ± 0.9 | - | 34.7 ± 1.3 | 45.3 ± 2.1 | 54.4 ± 2.2 |

*Because of technical issues day 4, the HunterLab MiniScan reading was not reported.

The SE for each day is assessed over a sample size of 24 (8 muscles × 3 positions).

DeoxyMb = deoxymyoglobin; MetMB = metmyoglobin; OxyMB = oxymyoglobin.

OxyMb and MetMb, as assessed by both DRS and HunterLab MiniScan spectrophotometer.

### *Daily changes of OxyMb, DeoxyMb, and MetMb forms as measured by DRS versus those by HunterLab MiniScan spectrophotometer*

The day-to-day averaging of the myoglobin redox forms of the 8 muscles over the duration of display are tabulated in Table 3 and presented as bar-plots in Figure 4. The upper panel of Figure 4, containing subplots (A), (B), and (C), was the result of DRS. The lower panel of Figure 4, containing subplots (D), (E), and (F), was the result of HunterLab MiniScan spectrophotometer while lacking the data on day 4. The OxyMb measured by DRS is shown in (A) and by HunterLab MiniScan spectrophotometer in (D). The DeoxyMb measured by DRS is shown in (B) and by HunterLab MiniScan spectrophotometer in (E). The MetMb measured by DRS is shown in (C) and by HunterLab MiniScan spectrophotometer in (F). The OxyMb, DeoxyMb, and MetMb are all displayed at the same scale from 0% to 100%, with the standard deviation overlapping on the bar representing the corresponding average.

These bar charts suggest the following trends of the muscle discoloration:

1. The OxyMb estimated by DRS decreased gradually over the duration of display. OxyMb estimated by DRS was 78.4% ± 13.3% on day 0 and reduced to 25.3% ± 13.5% on day 7. The OxyMb levels estimated by HunterLab MiniScan spectrophotometer changed unremarkable over the first 4 days and decreased apparently over the last 3 days of display. Overall, the OxyMb estimated by HunterLab MiniScan spectrophotometer was 83.5% ± 2.1% on day 0 and reduced to 33.1% ± 17.0% on day 7.
2. The DeoxyMb estimated by DRS remained relatively stable over day 0 to day 3 whereas it increased slightly over the remaining days. DeoxyMb estimated by DRS was 14.3% ± 7.3% on day 0 and increased to 20.1% ± 9.8% on day 7. The DeoxyMb levels estimated by HunterLab MiniScan spectrophotometer varied over the days of display, starting at 3.0% ± 2.2% on day 0 and increasing to 10.5% ± 7.7% on day 7.
3. The MetMb estimated by DRS increased gradually over the days of display. MetMb estimated by DRS was 7.4% ± 6.2% on day 0 and increased to 54.7% ± 7.7% on day 7. The MetMb levels estimated by HunterLab MiniScan spectrophotometer increased apparently over the initial 4 days and the last 3 days of display. MetMb estimated by HunterLab MiniScan spectrophotometer was 6.6% ± 3.1% on day 0 and 23.6% ± 4.8% on day 4 and increased to 54.4% ± 11.3% on day 7.

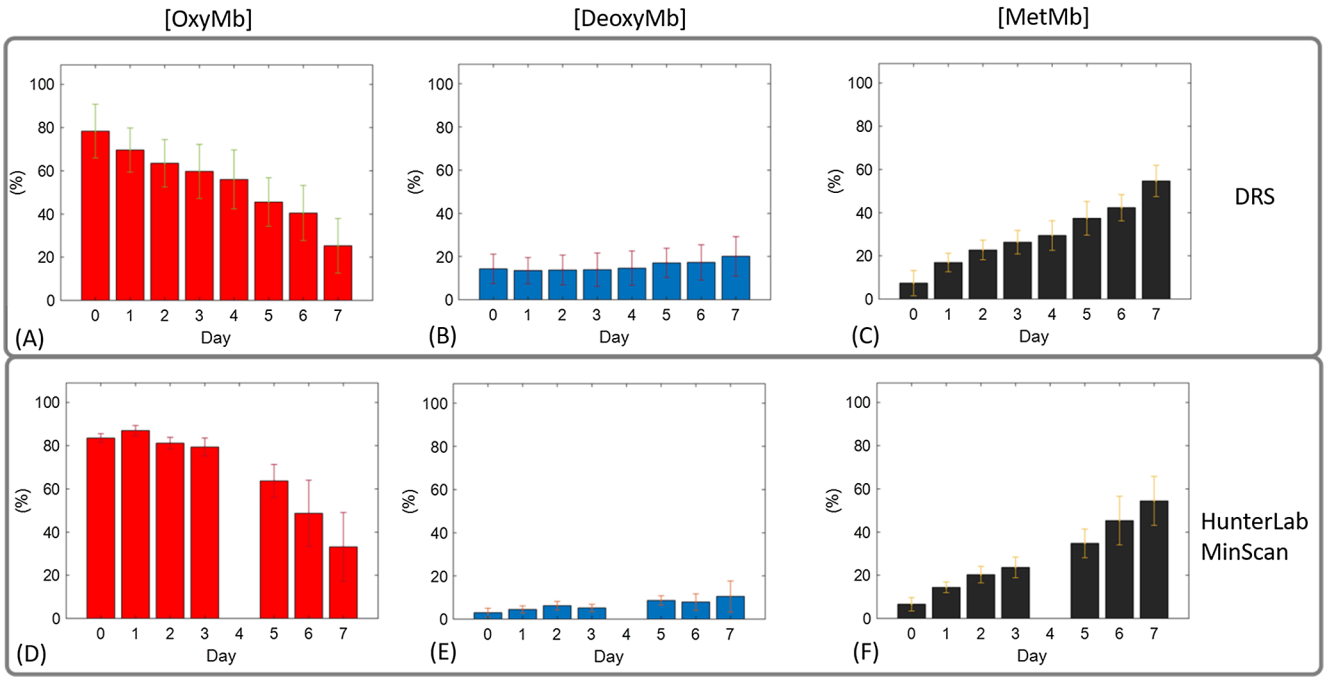


**Figure 4.** Longitudinal changes of OxyMb, DeoxyMb, and MetMb averaged for the 8 muscles over the duration of display. The upper panel consisting of subplots (A), (B), and (C) was the result of DRS. The lower panel consisting of subplots (D), (E), and (F) was the result of HunterLab. On each sub-figure, the bar plots the average with the standard deviation indicated. OxyMb change is depicted in (A) and (D), DeoxyMb change is depicted in (B) and (E), and MetMb change is depicted in (C) and (F). All traits, including OxyMb, DeoxyMb, and MetMb, are displayed at the same scale corresponding to 0%–100%.

### *Correlations of measurements between DRS and HunterLab MiniScan spectrophotometer for OxyMb, DeoxyMb, and MetMb changes over the duration of display*

The myoglobin redox forms of the 8 muscles measured from day 0 to day 4 and from day 5 to day 7 by DRS are scatter-plotted in Figure 5 against those measured by HunterLab MiniScan spectrophotometer to assess the correlation between the 2 modalities on the same respective form of myoglobin. The measurements by DRS on day 4 were excluded because of the lack of the counterpart by HunterLab MiniScan spectrophotometer. Each plot thus contains 56 data points (8 muscles × 7 d), plotted by assigning the

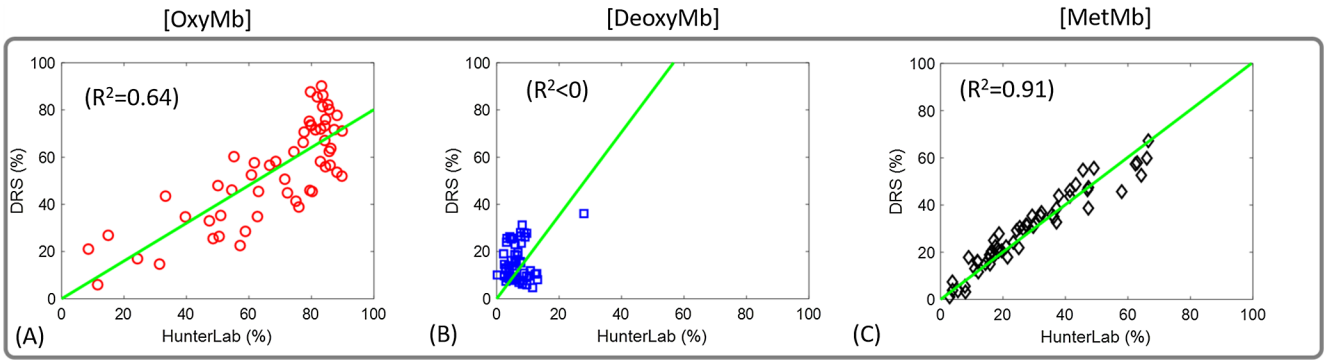


**Figure 5.** Correlation of a myoglobin form between that estimated by DRS and that estimated by HunterLab. Each subfigure contained 56 measurements corresponding to 8 samples × 7 days. The measurement by HunterLab serves as the abscissa, and the estimation by DRS plots as the ordinate. (A) shows the correlation of OxyMb as measured by the 2 modalities, which returns a slop of 0.802 that corresponds to an error of −19.8% of the NIR-DRS reading with respect to the reference measurement by HunterLab MiniScan spectrophotometer. (B) Shows the correlation of DeoxyMb as measured by the 2 modalities, which returns a slope of 1.766 that corresponds to an error of 76.6% of the NIR-DRS reading with respect to the reference measurement by HunterLab MiniScan spectrophotometer. (C) Shows the correlation of MetMb as measured by in (C) the 2 modalities. On each subplot, the green line represents a linear regression to the scattered data with a zero interception of the line with the abscissa, which returns a slope of 1.004 that corresponds to an error of 0.4% of the NIR-DRS reading with respect to the reference measurement by HunterLab MiniScan spectrophotometer. All traits, including OxyMb, DeoxyMb, and MetMb, are displayed at the same scale corresponding to 0%–100%.

measurements of HunterLab MiniScan spectrophotometer as the abscissa and the measurements of DRS as the ordinate. All 3 plots are displayed at the same scale of 100% over both abscissa and ordinate. A linear regression with a forced zero interception onto the ordinate is performed to obtain the slope and a regression measure of $R^2$. The slope represents how accurate the predictive change of the NIR-DRS reading has been with respect to the reference values rendered by HunterLab MiniScan spectrophotometer. A slope of exactly 1.00 corresponds to an exact match or 100% accurate prediction of the NIR-DRS reading when compared with the reference values established by HunterLab MiniScan spectrophotometer. A slope of 0.95 or 1.05 would then correspond to a 5% error of prediction of the NIR-DRS readings when compared with the reference measurements from the HunterLab MiniScan spectrophotometer. The plot for OxyMb returned (1) a slope of 0.802 that corresponds to an error of underestimation of −19.8% by the NIR-DRS reading with respect to the reference measurement by HunterLab MiniScan spectrophotometer and (2) a regression of $R^2 = 0.64$ indicating moderate correlation between the measurements by DRS and those by HunterLab MiniScan spectrophotometer. The plot for DeoxyMb returned (1) a slope of 1.766 that corresponds to an error of overestimation of 76.6% by the NIR-DRS reading with respect to the reference measurement by HunterLab MiniScan spectrophotometer and (2) a regression of $R^2 < 0$ indicating no apparent correlation between the measurements by DRS and those by HunterLab MiniScan spectrophotometer. The plot for MetMb returned (1) a slope of 1.004 that corresponds to an error of overestimation of only 0.4% of the NIR-DRS reading with respect to the reference measurement by HunterLab MiniScan spectrophotometer and (2) a regression of $R^2 = 0.91$ suggesting a strong correlation between the measurements by DRS and those by HunterLab MiniScan spectrophotometer. Note that the linear fit with a forced zero interception in (C) for MetMb that nearly coincided with the diagonal line signifies that the MetMb proportion estimated by DRS is nearly identical to that estimated by HunterLab MiniScan spectrophotometer.

## *Methodological aspect of the present approach in the context of meat color assessment*

The currently established commercial or experimental methods to quantify the myoglobin redox forms on muscle by using light of spectral nature may be classified into 2 categories as schematically compared in Figure 6. The comparison is based primarily on the relative position of the light remission/collection site with respect to the site/area of light illumination on the muscle surface. The first category corresponds to the site of light remission/collection that overlaps with the area of light illumination. This configuration can be implemented by applying light to the muscle over a broad aperture to form essentially a diffuse illumination and acquiring the light that has propagated in muscle (thus informing the muscle absorption and scattering) and remitted from muscle surface over a small aperture dictated by the collection optics. The light acquired by such a configuration usually has only sampled very shallow layers of muscle, on the orders of a few to a few hundred microns, as the light remission is dominated by the shallow-sampling component. The spectral intensity of the light as a function of the muscle absorption and scattering—i.e., the outcome of light–tissue interaction—corresponding to such a geometry of diffuse illumination and collimated collection must then be analyzed by mathematical models for the redox forms to be estimated.

The approach shown as (A) converts the diffuse surface reflectance to the wavelength-dependent KM function. The approach shown as (B) converts the diffuse surface reflectance to a wavelength-dependent absorbance. The approach of (B) differs from the approach of (A) in primarily the mathematical model used to transform the spectral diffuse reflectance to the final percentage representation of the myoglobin redox forms.

The approach shown in (C), introduced by Mohan et al. (2010a), was unique because it was based on frequency-domain (FD) near-infrared spectroscopy at 2 wavelengths of 630 nm and 830 nm. The operating principle of FD near-infrared spectroscopy is that, as a light of intensity modulation at the order of 100 MHz is sent to the muscle, the scattering of the light by muscle causes a phase-shift of the light comparing to a light taking a ballistic path. The phase-shift of the intensity-modulated light is measurable by separating the illumination site and detection site on the muscle surface (over a minimal of 2 cm as shown) to allow the scattering-caused phase-shift to build up to the level of being detectable. This scattering-carrying phase shift that is measured by way of frequency-modulated light allows accurate measurement (isolation) of the muscle absorption from the muscle attenuation of light. The minimal source-detector separation of 2 cm corresponds to a sampling depth of approximately 1 cm of the so-called “banana-shaped” region to which the

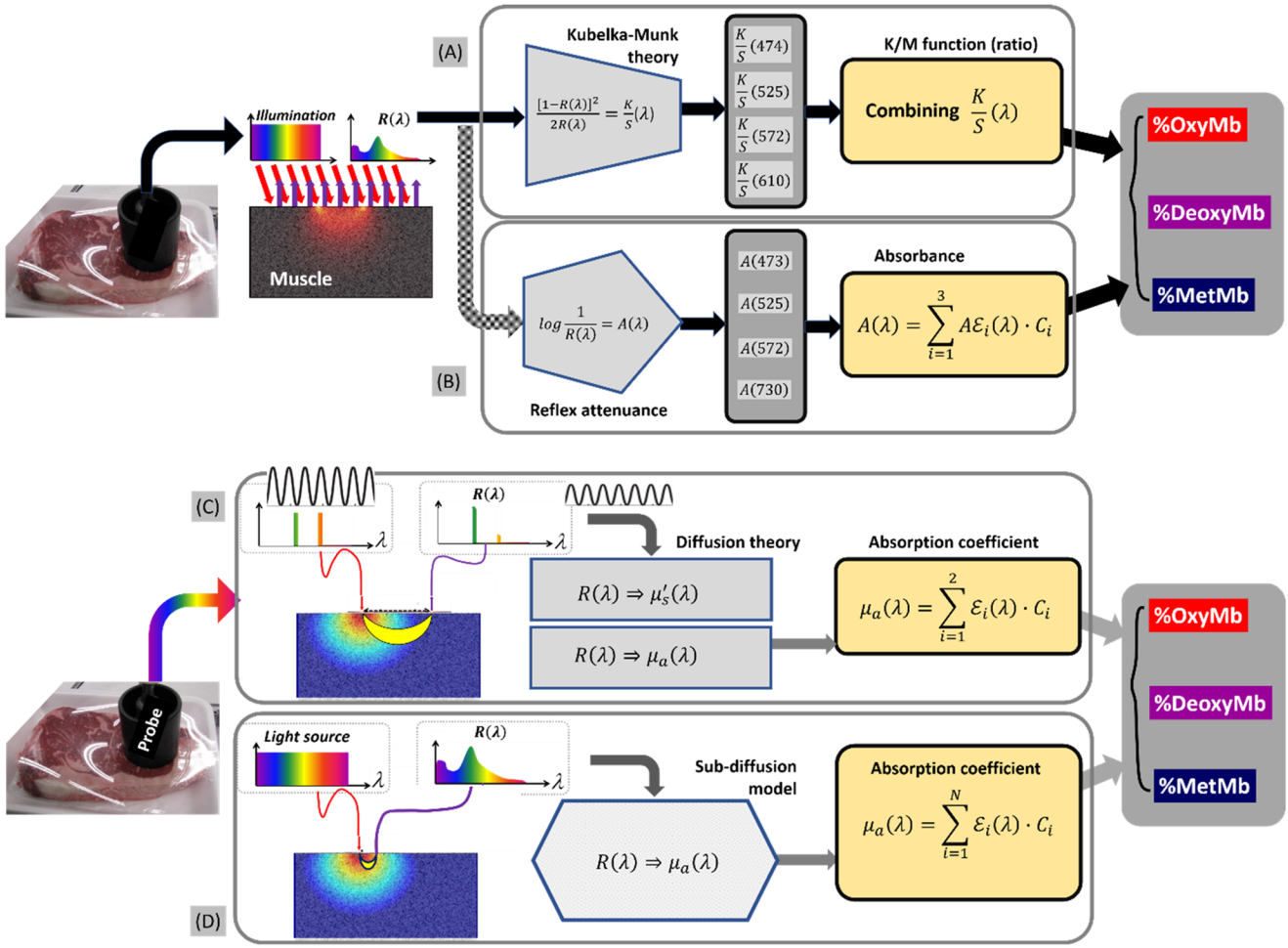


**Figure 6.** Schematic differences of approaches used for assessing myoglobin redox forms. The upper panel containing (A) and (B) compares the approaches falling in the guidelines of AMSA. The lower panel containing (C) and (D) compares the approaches that have been demonstrated by Mohan et al. (2010a) and this present work. (A) Refers to the use of KM theory to recover KM functions or ratios at 4 isosbestic wavelengths, with which the myoglobin redox forms are calculated. (B) Refers to the assumption of reflectance attenuance to recover absorbance at 4 isosbestic wavelengths to calculate the myoglobin redox forms. (C) A method of FD near-infrared spectroscopy demonstrated by Mohan et al. (2010a), which uses intensity modulated light at 2 wavelengths to probe muscle scattering to help resolve muscle absorption at the 2 wavelengths, from which the 2 forms of myoglobin can be quantified. (D) The method of the present method, which uses continuous-wave broad-band light with a source-detector separation allowing sampling muscle at a depth much deeper than that of (A) and (B), yet substantially smaller than that of (C) wherein the light at 2 wavelengths were intensity modulated.

measurement is sensitive. The >1 cm source-detector separation makes it feasible to treat the sub-surface propagated light as completely diffused when detected to recover tissue absorption and scattering properties from the surface measurement. The use of light modulation or FD technology is advantageous for recovering the pure absorption information; however, the need to modulate light at the high frequency limited the numbers of wavelengths to 2 values. The pure absorption at the 2 wavelengths allowed recovering the OxyMb and DeoxyMb, and with more constraints on the spectral recovery, the MetMb proportion was also obtained (Mohan et al., 2010b).

The approach shown in (D) illustrated the NIR-DRS demonstrate in this work and how it may differ from all 3 methods referred to heretofore. The present approach differs from the approaches of (A) and (B) in 2 aspects: (1) the source-detector arrangement affecting the sampling depth and (2) the mathematical models governing the conversion of the surface measured diffuse reflectance to the myoglobin redox forms. The present approach differs from the approach of (C) in the following aspects: (1) a broad-band light source is used in comparison to laser light operated at only 2 wavelengths; (2) continuous-wave light is applied, i.e., the light intensity is not modulated; and (3) the source-detector separation was only 3 mm, which is approximately one order of magnitude shorter. This much shorter source-detector distance required to customize light–tissue interaction model to address light propagation in a subdiffusive domain, which is less known than a diffusive region, as in (C). The 3-mm

source-detector separation facilitated a sampling depth of approximately 1.5 mm, which is much smaller than that of (C), albeit substantially deeper than those accessible by the methods of (A) and (B).

The current work was conducted on beef packaged in PVC manifesting changes in the levels of OxyMb, DeoxyMb, and MetMb over the duration of display. We have seen a strong correlation of the MetMb changes between those measured by NIR DRS and those measured by HunterLab MiniScan spectrophotometer. MetMb increased gradually over the days of display when measured by both methods. This gradual, monotonic increase of MetMb was consistent with what could be expected in association with the gradual decrease of OxyMb as measured by NIR-DRS. The OxyMb measured by HunterLab MiniScan spectrophotometer, however, did not show as much of the level of decrease at the first few days. This lower level of association of the OxyMb changes between the 2 methods is corroborated by the lack of correlation of the DeoxyMb between the 2 methods. We note that a few readings of negative DeoxyMb values were given by using the HunterLab MiniScan spectrophotometer. This may be attributable to the inadequate wavelength specificities of the 4 wavelengths to OxyMb, DeoxyMb, and MetMb. For example, the double-peaks of absorption of OxyMb between 540 and 580 nm are separated by the single absorption peak of DeoxyMb at 560 nm. At inadequate spectral resolution, such as 10 nm, the spectral changes over 540 to 580 nm may become smoothed by the combined spectral absorptions by OxyMb and MetMb that could make the spectral recovery somewhat ambiguous. The ambiguity of spectral recovery could be mitigated with the use of more wavelengths to make the number of measurements (wavelengths) exceeding the number of unknowns (myoglobin forms). In our case, the number of wavelengths used was 18, a number much greater than the 3 redox forms of myoglobin. This made the estimation of the myoglobin redox forms an overestimated problem that helped avoid readings of negative values for DeoxyMb.

The reflectance measurements rendered by HunterLab MiniScan spectrophotometer were limited to assessing the surface myoglobin redox forms and therefore were incapable of providing much insight into pigment dynamics in the depths of the meat (Mohen et al 2010a, 2010b). Our measurements of the myoglobin redox forms by using NIR-DRS that sampled approximately 1.5 mm in depth was in agreement with the report by Behrends (2004) regarding the decrease in the oxygen penetration depth of muscle during display. The ability to assess myoglobulin redox forms at a depth greater than is available by current technologies represented by the HunterLab MiniScan spectrophotometer could, in the future, facilitate more accurate assessment of oxygen consumption altering the penetration of oxygen into the muscle for more accurate prediction of discoloration of the shelf life of muscle for consumer value.

A limitation of our approach is the lack of consideration of the spectral variation of scattering in the mathematical model that converts the spectral reflectance to the tissue attenuation from which the total spectral absorption was deduced for spectral decomposition. Technologies such as the FD approach used by Mohan et. al. (2010a) may be necessary to accurately determine the wavelength-dependent scattering of muscle. To apply the FD approach for the entire spectra of intertest as explored in this work would be quite challenging. Alternatively, the scattering of soft tissue like muscle in the visible/NIR range is known to follow a simple pattern approximated by a power law that is consistent with Mie-scattering (Wang et al., 2005). Future work would be directed to address such approaches that may help account for the scattering variation of muscle to resolve the pure absorption spectral changes caused by the redox forms of myoglobin.

## Conclusions

NIR-DRS was used to monitor OxyMb, DeoxyMb, and MetMb on beef *longissimus lumborum* muscles during 7-d retail display. The in-house developed NIR-DRS system allowed for sampling of myoglobin redox forms in muscle, at 18 wavelengths, over a sampling depth that reached approximately 1.5 mm. Myoglobin redox forms developing in 8 PVC-packaged beef *longissimus lumborum* steaks over 7 d of retail display were measured. Daily assessment of the myoglobin redox forms from the 8 muscles were conducted using NIR-DRS in comparison with those assessed by HunterLab MiniScan spectrophotometer. Data for both methods showed high correlation ($R^2 = 0.91$) for MetMb changes, moderate correlation ($R^2 = 0.64$) for OxyMb changes, and lack of correlation for DeoxyMb changes over the duration of display. MetMb was shown by both measurements to have increased steadily over the duration of display. Comparatively, whereas DRS revealed OxyMb to have decreased steadily over the duration of display, HunterLab MiniScan spectrophotometer indicated a later onset of the apparent decrease of OxyMb over the

duration of display. DRS has potential as an alternative method of color assessment in postrigor skeletal muscle.

## Literature Cited


AMSA. 2012. Meat Color Measurement Guidelines. American Meat Science Association, Champaign, IL.

Behrends, J. M. 2004. Metmyoglobin reducing ability and visual characteristics of nine selected bovine muscles. Texas A&M University, College Station, TX.

Bowen, W. J. 1949. The absorption spectra and extinction coefficients of myoglobin. J. Biol. Chem. 179:235–245.

Davis, M. L., and T. J. Barstow. 2013. Estimated contribution of hemoglobin and myoglobin to near infrared spectroscopy. Resp. Physiol. Neurobi. 186:180–187. https://doi.org/10.1016/j.resp.2013.01.012.

de Groot, B., C. J. Zuurbier, and J. H. van Beek. 1999. Dynamics of tissue oxygenation in isolated rabbit heart as measured with near-infrared spectroscopy. Am. J. Physiol. 276:H1616–H1624. https://doi.org/10.1152/ajpheart.1999.276.5.H1616.

Hernandez, B., C. Saenz, C. Alberdi, and J. M. Dineiro. 2015. Comparison between two different methods to obtain the proportions of myoglobin redox forms on fresh meat from reflectance measurements. J Food Sci Technol 52:8212–8219. https://doi.org/10.1007/s13197-015-1917-x.

Hughes, J., F. Clarke, Y. Li, P. Purslow, and R. Warner. 2019. Differences in light scattering between pale and dark beef longissimus thoracis muscles are primarily caused by differences in the myofilament lattice, myofibril and muscle fibre transverse spacings. Meat Sci. 149:96–106. https://doi.org/10.1016/j.meatsci.2018.11.006.

Hughes, J., F. Clarke, P. Purslow, and R. Warner. 2017. High pH in beef longissimus thoracis reduces muscle fibre transverse shrinkage and light scattering which contributes to the dark colour. Food Res. Int. 101:228–238. https://doi.org/10.1016/j.foodres.2017.09.003.

Hunt, M. C., J. C. Acton, R. C. Benedict, C. R. Calkins, D. P Cornforth, L. E. Jeremiah, D. G. Olson, C. P. Salm, J. W. Savell, and S. D. Shivas. 1991. Guidelines for meat color evaluation. AMSA Committee on Guidelines for Meat Color Evaluation. National Livestock and Meat Board, Chicago, Illinois.

Kubelka, P. 1948. New contributions to the optics of intensely light-scattering materials. J. Opt. Soc. Am. A. 38:448–57. https://doi.org/10.1364/josa.38.000448.

Mancini, R. A., and M. C. Hunt. 2005. Current research in meat color. Meat Sci. 71:100–121. https://doi.org/10.1016/j.meatsci.2005.03.003.

Mohan, A., M. C. Hunt, T. J. Barstow, T. A. Houser, C. Bopp, D. M. Hueber. 2010a. Effects of fibre orientation, myoglobin redox form, and postmortem storage on NIR tissue oximeter measurements of beef longissimus muscle. Meat Sci. 84:79–85. https://doi.org/10.1016/j.meatsci.2009.08.024.

Mohan, A., M. C. Hunt, T. Barstom, T. A. Houser, and D. M. Hueber. 2010b. Near-infrared oximetry of three post-rigor skeletal muscles for following myoglobin redox forms. Food Chem. 123:456–464. https://doi.org/10.1016/j.foodchem.2010.04.068.

Molenaar, R., J. J. ten Bosch, and J. R. Zijp. 1999. Determination of Kubelka-Munk scattering and absorption coefficients by diffuse illumination. Appl. Optics. 38:2068–2077. https://doi.org/10.1364/ao.38.002068.

Mourant, J. R., O. C. Marina, T. M. Hebert, G. Kaur, and H. O. Smith. 2014. Hemoglobin parameters from diffuse reflectance data. J. Biomed. Opt. 19:37004. https://doi.org/10.1117/1.JBO.19.3.037004.

Piao, D. 2019. Laparoscopic diffuse reflectance spectroscopy of an underlying tubular inclusion: a phantom study. Appl. Optics. 58:9689–9699. https://doi.org/10.1364/AO.58.009689.

Piao, D., H. Borron, A. Hawxby, H. Wright, E. M. Rubin. 2018. Effects of capsule on surface diffuse reflectance spectroscopy of the subcapsular parenchyma of a solid organ. J. Biomed. Opt. 23:1–23. https://doi.org/10.1117/1.JBO.23.12.121602.

Piao, D., and T. Sun. 2021. Diffuse photon remission from thick opaque media of the high absorption/scattering ratio beyond what is accountable by the Kubelka-Munk function. Opt. Lett. 46:1225–1228. https://doi.org/10.1364/OL.415650.

Purslow, P. P., R. D. Warner, F. M. Clarke, and J. M. Hughes. 2020. Variations in meat colour due to factors other than myoglobin chemistry; a synthesis of recent findings (invited review). Meat Sci. 159:107941. https://doi.org/10.1016/j.meatsci.2019.107941.

Ramanathan, R., M. C. Hunt, A. R. English, G. G. Mafi, and D. L. VanOverbeke. 2019. Effects of aging, modified atmospheric packaging, and display time on metmyoglobin reducing activity and oxygen consumption of high-pH beef. Meat Muscle Biol. 31:276. https://doi.org/10.22175/mmb2019.05.0017.

Sandoval, C., and A. D. Kim. 2014. Deriving Kubelka-Munk theory from radiative transport. J. Opt. Soc. Am. A. 31:628–636. https://doi.org/10.1364/JOSAA.31.000628.

Schmitt, J. M., and G. Kumar. 1998. Optical scattering properties of soft tissue: A discrete particle model. Appl. Optics. 37:2788–2797. https://doi.org/10.1364/ao.37.002788.

Sun, T., and D. Piao. 2019. Simple analytical total diffuse reflectance over a reduced-scattering-pathlength scaled dimension of [10(-5), 10(-1)] from a medium with HG scattering anisotropy. Appl. Optics. 58:9279–9289. https://doi.org/10.1364/AO.58.009279.

Swatland, H. J. 2008. How pH causes paleness or darkness in chicken breast meat. Meat Sci 80:396–400. https://doi.org/10.1016/j.meatsci.2008.01.002.

Tang, J., C. Faustman, and T. A. Hoagland. 2004. Krzywicki revisited: Equations for spectrophotometric determination of myoglobin redox forms in aqueous meat extracts. J. Food Sci. 69:C717–C720. https://doi.org/10.1111/j.1365-2621.2004.tb09922.x.

Wang, X., B. W. Pogue, S. Jiang, X. Song, K. D. Paulsen, C. Kogel, S. P. Poplack, W. A. Wells. 2005. Approximation of Mie scattering parameters in near-infrared tomography of normal breast tissue in vivo. J. Biomed. Opt. 10:051704. https://doi.org/10.1117/1.2098607.

Wilson, J. R., D. M. Mancini, K. McCully, N. Ferraro, V. Lanoce, and B. Chance. 1989. Noninvasive detection of skeletal muscle underperfusion with near-infrared spectroscopy in patients with heart failure. Circulation. 80:1668–1674. https://doi.org/10.1161/01.cir.80.6.1668.